Multilinear Modeling and Simulation of a Multi-stack PEM Electrolyzer with Degradation for Control Concept Comparison

Aline Luxa[1][a], Niklas Jöres[1][b], Carlos Cateriano Yáñez[1,2,3][c], Marina Nascimento Souza[1][d],
Georg Pangalos[1][e], Leona Schnelle[2][f] and Gerwald Lichtenberg[2][g]

[1]*Application Center for Integration of Local Energy Systems, Fraunhofer IWES, Hamburg, Germany*
[2]*Faculty of Life Science, HAW Hamburg, Germany*
[3]*Universitat Politècnica de València, Instituto Universitario de Automática e Informática Industrial, València, Spain*

Keywords: Multilinear Simulation, Energy Systems, PEM Electrolyzer, Multi-stack Operation, Controller Design, Degradation, Wind Energy.

Abstract: Hybrid energy systems, e.g., with wind energy and hydrogen production, have a high model complexity due to their multi-physics nature, which poses major control challenges for the optimization of plant operation. This work aims at addressing this issues by introducing a highly efficient modeling and simulation framework. A proton exchange membrane (PEM) electrolyzer stack, including degradation and controller, has been modeled using the multilinear class. This class enables the automatic append of individual models, which is used to stack a 100 multi-stack PEM electrolyzer model. Moreover, the multilinear class models can be represented as tensors, which allows for efficient decomposition methods and formats. This is used to considerably enhance the simulation performance of the system, making the simulation of a one year multi-stack electrolyzer operation possible, with a reasonable computational cost. In the simulation, two different high-level control modes are compared regarding overall degradation gain and electrolyzer efficiency. The developed modeling and simulation framework has proven its suitability for big-scale complex models, enabling efficient simulations for controller analysis.

1 INTRODUCTION

The transition of the energy system from centralized to local holds a variety of challenges, which can be tackled by model-based approaches. For this, simulation problems are getting larger with an enormous number of states. Therefore, innovative modeling methods are needed to be able to solve control and optimization tasks.

The future power grid will be constructed of a multitude of local energy systems. These are formed by combinations of renewable energy generation units, consumers, and energy storage systems. This results in a modeling problem for con-

[a] https://orcid.org/0000-0002-3025-3274
[b] https://orcid.org/0000-0003-2471-3892
[c] https://orcid.org/0000-0001-5261-2568
[d] https://orcid.org/0000-0003-2523-5669
[e] https://orcid.org/0000-0001-5094-8033
[f] https://orcid.org/0000-0002-2600-8110
[g] https://orcid.org/0000-0001-6032-0733

trolling numerous local energy system (LES). One possible composite of LES is a coupled wind park with electrolyzers for hydrogen production. According to the coalition agreement $2021\,to\,2025$, Germany has a 10 GW goal of electrolysis capacity until 2030. To achieve this goal, Germany would need to build several plants in the larger MW range, many of which are already being planned. Trianel and Stadtwerke Hamm signed a joined venture with the goal to install 20 MW electrolyzer capacity in the natural gas power plant Hamm-Uentrop by 2022. Shell, Mitsubishi Heavy Industries, Vattenfall and Wärme Hamburg signed a declaration of intent to build 100 MW installed capacity of electrolysis in the port of Hamburg, which is supposed to be in operation in 2025 (Geitmann, 2022).

In the near future, the mass production of proton exchange membrane (PEM) electrolysis stacks in the larger kW to MW range is expected. Systems of multiple GW capacity will be mostly composed of stacks between 1 and 2 MW (P. Ayivor et al., 2018). Therefore, electrolyzer systems with a nominal capacity in

the larger MW to GW area will be constructed of several hundred stacks. In a modular approach for a high power electrolysis system, stacks are usually connected in parallel or sometimes in series, which is then called string or cascade. Larger systems with smaller stacks are constructed with strings connected in parallel.

There are many stack manufactures that offer modular scale-up solutions, e.g., Green Hydrogen Systems (GHS) alkaline electrolyzer system is scalable up to 20 MW, while GHS current portfolio is offering options in the range from $125 to 390$ kW (Green Hydrogen Systems, 2022). Similarly, H-TEC SYSTEMS offers a PEM electrolyzer of 1 MW containing 9 stacks (H-TEC SYSTEMS GmbH, 2022). Enapter approaches the market with a highly modular anion exchange membrane (AEM) system with nominal capacity of 1 MW composed of 420 stacks (Enapter, 2022). Therefore, the modeling problem of control and operation optimization for the multi-stack electrolyzer (mELY) emerges.

When operating an mELY, there is the conflict between optimizing efficiency and stack lifetime. Gaining a higher efficiency by running more stacks in partial load conflicts with degradation of each stack, depending on the load. A central main controller has to decide between partial load operation and shutting down stacks completely to prevent aging. Therefore, electrolyzer degradation plays a special role in the modeling problem and cannot be neglected. The introduction of degradation models into control applications is known generally but is not yet done for mELY, to the best of the authors' knowledge (Zagorowska et al., 2020). It can be assumed that this is because suitable degradation models and powerful modeling approaches are missing.

Overall, the main purpose of the paper is building the base for the optimization of large controlled mELY systems considering stack degradation, by using the multilinear time-invariant (MTI) model class. The MTI model class, which current developments can be explored in (Lichtenberg et al., 2022), is a powerful modeling tool, when it comes to combining submodels of a system. The possible automatic model generation can be coupled with model reduction methods, for decreased complexity and increased simulation performance. With the MTI model approximation of nonlinear models, basic nonlinear phenomena are representable. Furthermore, the MTI models allow deterministic runtimes with a rank, that is increasing linearly, and not exponentially with the order of the system(Lichtenberg et al., 2022). Therefore, the MTI framework is chosen for the automatized combination of the submodels: electrolyzer,

electrolyzer controller, degradation, and main controller for renewable power distribution, for an arbitrary number of stacks. The modeling framework allows to later on substitute every submodel easily, if, e.g., degradation models develop further. The evaluation of the simulation results help to decide for different control schemes for mELY operation.

First, in section 2 multilinear modeling and the applied methods for model reduction are introduced. Afterwards, the used individual models are described in section 3, including the electrolyzer, electrolyzer controller, and degradation, which will be composed to the total single-stack electrolyzer (sELY) model. In section 4 the main controller model and the stacking for the mELY model composition is described. The section 5 contains a code to code validation of the stand alone MTI electrolyzer stack model approximation by comparing nonlinear, linear, and multilinear simulation results. Furthermore, the total mELY system is simulated with renewable power input from wind data. Afterwards, the analysis of the simulation results is executed in section 6. Finally, in section 7 the key findings are derived, and further steps are described for future work.

2 MULTILINEAR MODELING

In the following chapter, the explicit multilinear time-invariant (eMTI) model description will be introduced, which is an extension to the standard linear time-invariant (LTI) class. In contrast, to LTI the eMTI class allows for multiplication of states and/or inputs (Pangalos et al., 2013).

Explicit multilinear models are no universal approximators per se like other model classes (Hornik et al., 1989). However, they are able to model general polynomial dependencies by either extension of the state space (Kruppa, 2018) or using implicit forms (Lichtenberg et al., 2022). This chapter also includes the model reduction methods.

2.1 Multilinear Tensor Modeling

The state and output equations of an explicit multilinear model in tensor representation as introduced in (Pangalos et al., 2013; Lichtenberg et al., 2022) is given as

$$\dot{\mathbf{x}} = \langle\, \mathsf{F} \,|\, \mathsf{M}(\mathbf{x}, \mathbf{u}) \,\rangle \,, \qquad (1a)$$

$$\mathbf{y} = \langle\, \mathsf{G} \,|\, \mathsf{M}(\mathbf{x}, \mathbf{u}) \,\rangle \,, \qquad (1b)$$

where $\langle \sim | \sim \rangle$ denotes the contracted product, $\mathsf{F} \in \mathbb{R}^{\overbrace{2 \times \cdots \times 2}^{n+m} \times n}$ and $\mathsf{G} \in \mathbb{R}^{\overbrace{2 \times \cdots \times 2}^{n+m} \times l}$ contain the

parameters of the model and $M(\mathbf{x},\mathbf{u}) \in \mathbb{R}^{\overbrace{2 \times \ldots \times 2}^{n+m}}$ is the monomial tensor given in canonical polyadic (CP) decomposed form as

$$M(\mathbf{x},\mathbf{u}) = \left[\begin{pmatrix} 1 \\ x_1 \end{pmatrix}, \ldots, \begin{pmatrix} 1 \\ x_n \end{pmatrix}, \begin{pmatrix} 1 \\ u_1 \end{pmatrix}, \ldots, \begin{pmatrix} 1 \\ u_n \end{pmatrix} \right],$$

(2)

with number of states n, number of inputs m, and number of outputs l. An example for $n = 2$ and $m = 1$ is given as

In case of full tensors, the contracted product is calculated as illustrated by the following example for a tensor $X \in \mathbb{R}^{2 \times 2 \times 3}$ and a tensor $Y \in \mathbb{R}^{2 \times 2}$. To calculate the contracted product $Z = \langle X \, | \, Y \rangle \in \mathbb{R}^3$, the matching dimensions, which are highlighted in red, have to be multiplied element-wise

The element-wise multiplication is shown exemplarily for z_1 as

$$z_1 = x_{111}y_{11} + x_{121}y_{12} + x_{211}y_{21} + x_{221}y_{22} .$$

(3)

To calculate the state update, when the model is in CP tensor form with parameter tensors given as

$$F = \left[\mathbf{F}_{x_1}, \ldots, \mathbf{F}_{x_n}, \mathbf{F}_{u_1}, \ldots, \mathbf{F}_{u_m}, \mathbf{F}_\phi \right],$$ (4a)
$$G = \left[\mathbf{G}_{x_1}, \ldots, \mathbf{G}_{x_n}, \mathbf{G}_{u_1}, \ldots, \mathbf{G}_{u_m}, \mathbf{G}_\phi \right],$$ (4b)

the contracted product simplifies to

$$\dot{\mathbf{x}} = \mathbf{F}_\phi \left(\left(\mathbf{F}_1^\mathsf{T} \begin{pmatrix} 1 \\ x_1 \end{pmatrix} \right) \circledast \cdots \circledast \left(\mathbf{F}_n^\mathsf{T} \begin{pmatrix} 1 \\ x_n \end{pmatrix} \right) \circledast \right.$$
$$\left. \left(\mathbf{F}_{n+1}^\mathsf{T} \begin{pmatrix} 1 \\ u_1 \end{pmatrix} \right) \circledast \cdots \circledast \left(\mathbf{F}_{m+n}^\mathsf{T} \begin{pmatrix} 1 \\ u_m \end{pmatrix} \right) \right),$$ (5a)

$$\mathbf{y} = \mathbf{G}_\phi \left(\left(\mathbf{G}_1^\mathsf{T} \begin{pmatrix} 1 \\ x_1 \end{pmatrix} \right) \circledast \cdots \circledast \left(\mathbf{G}_n^\mathsf{T} \begin{pmatrix} 1 \\ x_n \end{pmatrix} \right) \circledast \right.$$
$$\left. \left(\mathbf{G}_{n+1}^\mathsf{T} \begin{pmatrix} 1 \\ u_1 \end{pmatrix} \right) \circledast \cdots \circledast \left(\mathbf{G}_{m+n}^\mathsf{T} \begin{pmatrix} 1 \\ u_m \end{pmatrix} \right) \right),$$ (5b)

where $\circledast$ denotes the element-wise or Hadamard product.

2.2 Reduction of Simulation Complexity

To reduce simulation complexity, the transition tensors F and G can be approximated using tensor decomposition methods. The decomposition can be performed by using the alternating least squares algorithm (Kolda, 2006). In general, low values for the ranks r_F and r_G are desired. However, a trade-off can be between the rank and the approximation error. Adequate values for r_F and r_G can be determined by a parameter study, comparing the results of the minimum possible rank for a solution of the optimization and higher ranks until the error is acceptable (Bro and Kiers, 2003). The approach on how to perform the CP decomposition for MTI models is explained in (Pangalos et al., 2013; Lichtenberg et al., 2022).

The CP decomposed parameter tensor, as shown in (4), can be normalized by applying different normalization methods to the columns of the factor matrices $\mathbf{F}_i, i = x_1, \ldots, x_n, u_1, \ldots, u_m, \phi$ as shown in (Lichtenberg et al., 2022) for 1-norm and in (Schnelle et al., 2022) for the euclidean 2-norm. The normalized parameter tensor

$$\widetilde{F} = \left[\widetilde{\mathbf{F}}_{x_1}, \ldots, \widetilde{\mathbf{F}}_{x_n}, \widetilde{\mathbf{F}}_{u_1}, \ldots, \widetilde{\mathbf{F}}_{u_m}, \widetilde{\mathbf{F}}_\phi \right] \in \mathbb{R}^{\overbrace{2 \times \ldots \times 2}^{n+m} \times n},$$ (6)

is defined by normalized factor matrices $\widetilde{\mathbf{F}}_i \in \mathbb{R}^{2 \times r}$ with $i = 1 \ldots n+m$, rank r, and $\widetilde{\mathbf{F}}_\phi \in \mathbb{R}^{n \times r}$ with arbitrary values.

With the so called sparse-norm, the columns of the factor matrices of the not normalized CP tensor F were normalized to their first elements such that all first elements get fixed to one. This leads to a normalized representation where only the second elements need to be stored in a vector

$$\tilde{\mathbf{f}}_i = \left(\frac{f_{2,1}}{f_{1,1}}, \frac{f_{2,2}}{f_{1,2}}, \cdots, \frac{f_{2,r}}{f_{1,r}} \right) \in \mathbb{R}^{1 \times r},$$ (7)

where $f_{1,j} \in \mathbb{R}\backslash\{0\}$, with $j = 1 \cdots r$. The vectors can

be stored in a matrix

$$\widetilde{\mathbf{F}} = \begin{pmatrix} \tilde{\mathbf{f}}_{x_1} \\ \vdots \\ \tilde{\mathbf{f}}_{x_n} \\ \tilde{\mathbf{f}}_{u_1} \\ \vdots \\ \tilde{\mathbf{f}}_{u_m} \end{pmatrix} = \begin{pmatrix} \widetilde{\mathbf{F}}_{\mathbf{x}} \\ \widetilde{\mathbf{F}}_{\mathbf{u}} \end{pmatrix} \in \mathbb{R}^{(n+m) \times r}, \qquad (8)$$

and the MTI model is fully defined by this matrix and

$$\widetilde{\mathbf{F}}_{\phi} = \mathbf{F}_{\phi} \circledast (\lambda_1, \lambda_2, \dots, \lambda_r) \in \mathbb{R}^{n \times r}, \qquad (9)$$

by element-wise multiplication with the weights of normalization $\lambda_j = \prod_{i=1}^{n+m} \mathbf{F}_i(1, j)$.

3 SINGLE-STACK ELECTROLYZER MODELING

In this section all individual submodels for the sELY combination will be described, followed by their composition. Later on, the sELY units will be stacked to build the total system for mELY simulation. The shown example is a purely continuous-time problem with all real variables. The current approach is restricted to models with concentrated parameters described by ordinary differential equations (ODE) and not distributed parameters described by partial differential equations (PDE).

3.1 Electrolyzer Model

For this paper, a 46 kW PEM electrolyzer model from literature is used to demonstrate the combination of the subsystems in eMTI format for large mELY operations (Espinosa-López et al., 2018). The nonlinear model is built up in MATLAB/Simulink, which is the base for the eMTI approximation, generated by the projection method (Kruppa et al., 2014). The thermal dynamic electrolyzer model has two states, i.e., temperature T and cooling power state x_{PI}, two inputs, i.e., current i_{ely} and membrane degradation r_{d}, and two outputs, i.e., voltage v_{ely} and stack efficiency η_{ely}. Thus, the state, input and output vectors are

$$\mathbf{x} = \begin{pmatrix} T \\ x_{\mathrm{PI}} \end{pmatrix}, \mathbf{u} = \begin{pmatrix} i_{\mathrm{ely}} \\ r_{\mathrm{d}} \end{pmatrix}, \mathbf{y} = \begin{pmatrix} v_{\mathrm{ely}} \\ \eta_{\mathrm{ely}} \end{pmatrix}. \qquad (10)$$

The ODE for describing the thermal dynamic states are introduced in the following. The temperature change is described by

$$\frac{\mathrm{d}T}{\mathrm{d}t} = \frac{1}{C_{\mathrm{th}}} \left(\sum_{k=1}^{z_1} \dot{W}_{\mathrm{k}} + \sum_{k=1}^{z_2} \dot{Q}_{\mathrm{k}} + \sum_{k=1}^{z_3} \dot{H}_{\mathrm{k}} \right), \quad (11)$$

with z_1 power $\dot{W}$, z_2 heat $\dot{Q}$ and z_3 enthalpy $\dot{H}$ streams, and the lumped thermal capacity C_{th} (Espinosa-López et al., 2018). As introduced in (Lichtenberg et al., 2022), the cooling heat $\dot{Q}_{\mathrm{cool}}$ is directly controlled by a PI controller, with state space model

$$\dot{Q}_{\mathrm{cool}} = x_{\mathrm{PI}} + K_{\mathrm{P}} \Delta T, \qquad (12\mathrm{a})$$

$$\frac{\mathrm{d}x_{\mathrm{PI}}}{\mathrm{d}t} = K_{\mathrm{I}} \Delta T. \qquad (12\mathrm{b})$$

The electrolyzer efficiency is defined as

$$\eta_{\mathrm{ely}} = \frac{\dot{n}_{\mathrm{H}_2} H_{\mathrm{s}}}{p_{\mathrm{ely}}}, \qquad (13)$$

containing the higher heating value of hydrogen H_{s} and the output hydrogen molar stream $\dot{n}_{\mathrm{H}_2}$, which is defined in (Espinosa-López et al., 2018). For calculations of the electrolyzer voltage, cathode activation overpotential and mass transfer losses are neglected. Therefore, the equation reduces to

$$v_{\mathrm{ely}} = v_{\mathrm{ocv}} + v_{\mathrm{ohm}} + v_{\mathrm{act-an}}, \qquad (14)$$

including the open circuit voltage v_{ocv}, ohmic overpotential v_{ohm}, and anode activation overpotential $v_{\mathrm{act-an}}$ (Espinosa-López et al., 2018).

For performing a multilinearization, an operating range needs to be defined for the application. PEM electrolyzers can be operated in overload for some time, which is mostly limited by the thermal management (Kopp et al., 2017). Also, there could be a restriction regarding a minimum load, which is influenced by the power consumption of ancillary components. This would add a boolean state variable for the electrolyzer operation for actually being turned on or off. In mELY operation, running below minimum load can mostly be prevented by completely turning off stacks and shifting the power to different ones. Allowing minimum or overload operation would therefore add another two boundary conditions to the main controller introduced in subsection 4.1. Nevertheless, for this demonstration there is no benefit in this, since the degradation model cannot yet include the effect of start-stop events. Therefore, the operating range is assumed to be $0 to 100$ % of the nominal load p_{nom} of 46 kW for each stack, at the state of begin of life (BoL) (no degradation). Even though the electrolyzer is only operated until 100 % load, the upper and lower bounds for multilinearization of the model using the projection method were determined with a load up to 150 % and 40 nodes. This was assumed to generate a higher accuracy at the nominal operation point. Due to limited space, the parameter tensors of the multilinear model of the electrolyzer are not shown here.

3.2 Electrolyzer Controller Model

Each electrolyzer stack has an individual integral feedback controller, which is tracking the error of the

power reference given by the main multi-stack controller and the current power of the stack, see Figure 2. A key feature of this controller is the multilinear term that calculates the current stack power. Thus the controller can not be represented as a linear system but as an MTI system. The stack controller can be expressed in CP representation as follows,

$$\mathsf{F}_{\text{ctrl}} = \left[\begin{pmatrix} 1 & 0 \\ 0 & 1 \end{pmatrix}, \begin{pmatrix} 0 & 1 \\ 1 & 0 \end{pmatrix}, \begin{pmatrix} 1 & 0 \\ 0 & 1 \end{pmatrix}, \begin{pmatrix} -K_{\text{I}} \\ K_{\text{I}} \end{pmatrix}^{\text{T}} \right],$$
(15a)

$$\mathsf{G}_{\text{ctrl}} = \left[\begin{pmatrix} 0 \\ 1 \end{pmatrix}, \begin{pmatrix} 1 \\ 0 \end{pmatrix}, \begin{pmatrix} 1 \\ 0 \end{pmatrix}, (1) \right],$$
(15b)

where $K_{\text{I}} = -1.28\mathrm{e}{-4}$ is the gain for the integrator.

3.3 Degradation Model

The current density, temperature, and pressure are factors that affect the PEM membrane electrode assembly (MEA) degradation mechanisms. Some of these mechanisms are: thinning of the membrane, decomposition of catalyst layer, and passivation of the porous transport layer (PTL). The mechanisms are caused by thermal and chemical stress, catalyst particle agglomeration at high temperature, dissolving of catalyst particles at high current densities, poisoning by metallic species, and oxidation of metals (Bahr et al., 2020). Separating the individual effects of each mechanism is very challenging. The study (Rakousky et al., 2017) reports degradation rates under different current densities, discovering catalyst degradation on the anode and increase of contact resistance at the titanium PTL as the two main degradation causes. In (Frensch et al., 2019) degradation rates under constant current and three different dynamic profiles are studied, concluding that anode catalyst degradation plays a minor role compared to ohmic resistance change. In (Bahr et al., 2020) a neural network application to describe the degradation rate is developed, by applying experimental results of accelerated aging tests to a data trained model. The study reports degradation rates according to current density and can be further developed with a broader database and under different temperature and pressure conditions. However, such a data-based model has no insight into changes of electrochemical parameters and rely on the experimental data. While predominant mechanisms have been investigated, up to date there is still no model for the description of aging due to fluctuant operation of PEM electrolysis.

In addition, stacks of an mELY system degradate at different rates according to the operation conditions. Therefore, the electrochemical model parameter of each stack can vary. As stated before, there are no generic phenomenological degradation models for PEM electrolyzers published, that can represent the influence on partial or dynamic load, as well as start-stop events. Nevertheless, for this work it is not essential to apply a degradation model that describes the electrochemical processes in detail. However, it will be demonstrated, how the degradation model can be integrated into the mELY system. The degradation model in this work is therefore to be considered as an estimate. It cannot be validated, as data over years of operation, even with accelerated aging tests, would be needed, which are currently non-existing. The combination of models establishes a basis to include more sophisticated degradation models to be developed later on.

The first assumption for the model is that the degradation only affects the membrane resistance (ohmic overpotential), and therefore just one electrochemical parameter. This is based on the findings of (Rakousky et al., 2017) and (Frensch et al., 2019) mentioned above, as well as on own experimental work, which is not published yet. To describe the variation of resistance, a total voltage drop rate, according to nominal operation time, is assumed. In (Buttler and Spliethoff, 2018) a rate of $4 \, to \, 8 \, \mu\mathrm{V}\,\mathrm{h}^{-1}$ is given, while $7 \, \mu\mathrm{V}\,\mathrm{h}^{-1}$ total degradation rate is given by (Kosonen et al., 2016). In this case $7 \, \mu\mathrm{V}\,\mathrm{h}^{-1}$ degradation rate at nominal load is used as base assumption. The overall degradation is fitted to the membrane resistance as displayed in Figure 1.
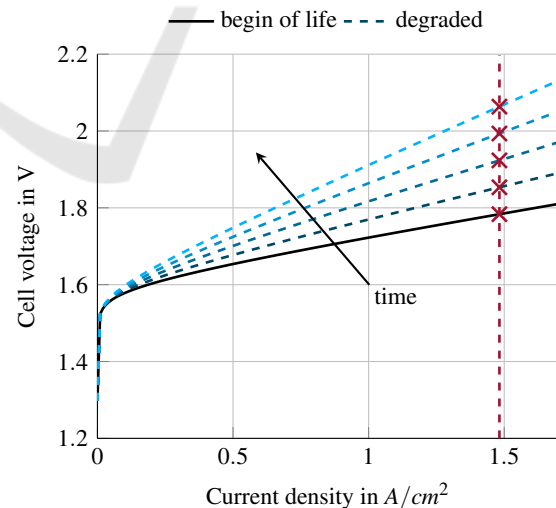

Figure 1: IV-curve fitted to total degradation at nominal load.

The single cell starting IV-curve (BoL) in Figure 1, which is not yet affected by degradation, is calculated by the base PEM electrolyzer model from (Espinosa-López et al., 2018) at 60 °C

and 35 bar cathode pressure. The aging process of $7\,\mu V\,h^{-1}$ is displayed at $1.48\,A\,cm^{-2}$ (46 kW at no degradation) for 10 years with 4000 full load hours (FLH) operation per year. The assumption of 10 years is a conservative lifetime estimation of different sources (Buttler and Spliethoff, 2018; IRENA, 2020; Cihlar et al., 2020) and at 4000 FLH green hydrogen gets cost competitive to fossil fuel based hydrogen (Agora Energiewende and Guidehouse, 2021).

As the voltage increases over time, the slope of the IV-curve changes, which can be fitted as displayed in Figure 1. The fit was done by an optimization, adjusting the slope of the IV-curve by changing r_d, until the degradation point was crossed. By this, the values for r_d until end of life (EoL) were estimated. The deviation of the description of v_{ohm} in (Espinosa-López et al., 2018) is implemented into the electrolyzer model as

$$v_{ohm} = (R_{mem} + r_d)i_{ely}. \tag{16}$$

In the following, the degradation resistance could be analyzed over time and fitted by a linear function, with a slope f_1 equal to the degradation rate. For the overall degradation model, the aging is assumed to be in linear proportion to the input current with 0 % at no load and 100 % of f_1 at nominal load. This leads to the general ODE description of

$$\frac{dr_d}{dt} = i_{ely}f_1. \tag{17}$$

The model for the degradation is linear and can therefore be formulated as eMTI model in CP representation as

$$\mathsf{F}_{deg} = \left[\begin{pmatrix} 1 \\ 0 \end{pmatrix}, \begin{pmatrix} 0 \\ 1 \end{pmatrix}, f_1 \right], \tag{18a}$$

$$\mathsf{G}_{deg} = \left[\begin{pmatrix} 1 & 0 \\ 0 & 1 \end{pmatrix}, \begin{pmatrix} 0 & 1 \\ 1 & 0 \end{pmatrix}, \begin{pmatrix} 1 & 0 \\ 0 & 1 \end{pmatrix} \right]. \tag{18b}$$

3.4 Series Composition of Models

The submodels will be connected in a series connection, which is described for eMTI models in (Lichtenberg et al., 2022). The block diagram in Figure 2 shows the single input, multiple output (SIMO) degradation and multiple input, single output (MISO) controller system in composition with the electrolyzer model. In further descriptions, the combination of the three models will be referred to as sELY.

The upper bound on the rank of the sELY model in CP form is $r_F = 12$ and $r_G = 13$. This can further be reduced by using the alternating least squares algorithm. A good approximation for the sELY was found with $r_F = 6$ and $r_G = 4$, which reduces the memory requirement by more than half.
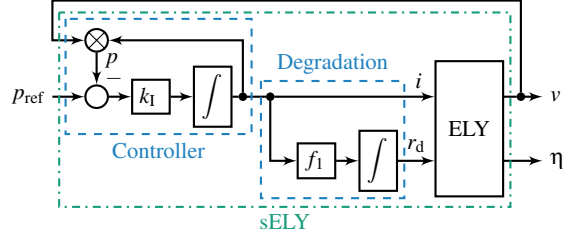

Figure 2: Scheme of the series connection of the electrolyzer controller, degradation and electrolyzer model.

4 MULTI-STACK ELECTROLYZER

For the mELY simulation, the main controller is creating the power input vector $\mathbf{p}_{ref}$ by distributing the total wind power. The sELY models are composed into one system and receive $\mathbf{p}_{ref}$ as input. The power distribution options and the composition method are described in the following.

4.1 Main Controller Model

The main mELY controller is a high-level controller with the principal objective of generating the power set point for each individual stack

$$\mathbf{p}_{ref} = \begin{pmatrix} p_{ref_1} \\ \vdots \\ p_{ref_N} \end{pmatrix}, \tag{19}$$

where $p_{ref_i} \geq 0$ for all $i \in [1, \cdots, N]$ and N is the number of stacks in mELY. Then $\mathbf{p}_{ref}$ is supplied as an input to mELY as seen in Figure 3.

There are two feedforward operation modes. In the base mode (mode 1 - equal), the wind power input data p_{wind} will be distributed equally to each stack, resulting in the same power reference

$$p_{ref}(t) = \min \left(p_{nom}, \frac{p_{wind}(t)}{N} \right), \tag{20}$$

for each unit. This is equivalent to a set of P controllers with the same gain for each stack, and a saturation to prevent values above the single stack nominal power p_{nom}. Here, the difference in the initial conditions of the degradation model of each stack, is expected to be the main driver for the overall mELY performance.

In the second mode (mode 2 - max), the power is distributed in such a way that the number of fully shut off stacks is maximized, while still providing the total requested power with the remaining online stacks.

This can be formulated as a minimization problem

$$\min_{\mathbf{p}_{\text{ref}}} \quad \sum_1^N \sigma\left(p_{\text{ref}_i}\right) r_{\text{d}0_i}, \qquad (21)$$

$$\text{s.t.} \quad \sum_1^N p_{\text{ref}_i} = \min\left(p_{\text{wind}}, N p_{\text{nom}}\right), \qquad (21a)$$

where σ is the Heaviside step function and $r_{\text{d}0_i}$ is the initial degradation of the ith stack.

This mode implies that almost all the remaining online stacks will be operating at nominal power, except when the total requested power is not a multiple of the nominal stack power, in which case one stack will need to take the remainder. In this strategy, the stacks with the lowest initial degradation will be selected first for nominal operation, such that the ones with the most initial degradation are shut off to improve the overall mELY efficiency.
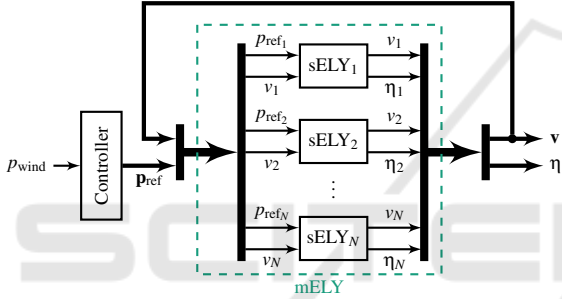

Figure 3: Multi-stack operation scheme.

4.2 Composition

For the connection of systems, three different options, i.e., series, parallel, and feedback have been introduced in (Lichtenberg et al., 2022).

In the case of an mELY, all subsystems can be fed with different amounts of power between minimum and maximum load. They work independently, without influencing each other, see Figure 3. Therefore, the sELY eMTI models are not connected in series, parallel or feedback, when considering an independent power supply for each unit. Hence, the append connector must be implemented for eMTI systems, which is grouping the submodels by appending their inputs and outputs (The MathWorks, Inc., 2022).

An eMTI model is fully defined with the normalized factor matrices $\widetilde{\mathbf{F}} \in \mathbb{R}^{(n+m)\times r}$ and the matrix $\widetilde{\mathbf{F}}_\phi \in \mathbb{R}^{n\times r}$. The append connector can then be applied easily by having the factor matrices of the individual stacks on the diagonal for the mELY

$$\widetilde{\mathbf{F}}_{\text{mELY}} = \begin{pmatrix} \widetilde{\mathbf{F}}_{\mathbf{x},1} & \mathbf{0}_{\mathbf{x}} & \cdots & \cdots & \cdots & \cdots\cdots & \mathbf{0}_{\mathbf{x}} \\ \mathbf{0}_{\mathbf{x}} & \ddots & \ddots & & & & \vdots \\ \vdots & \ddots & \ddots & \ddots & & & \vdots \\ \mathbf{0}_{\mathbf{x}} & \cdots & \mathbf{0}_{\mathbf{x}} & \widetilde{\mathbf{F}}_{\mathbf{x},N} & \mathbf{0}_{\mathbf{x}} & \cdots\cdots & \mathbf{0}_{\mathbf{x}} \\ \mathbf{0}_{\mathbf{u}} & \cdots\cdots & \mathbf{0}_{\mathbf{u}} & \widetilde{\mathbf{F}}_{\mathbf{u},1} & \mathbf{0}_{\mathbf{u}} & \cdots & \mathbf{0}_{\mathbf{u}} \\ \vdots & & & & \ddots & \ddots & \vdots \\ \vdots & & & & & \ddots & \ddots & \mathbf{0}_{\mathbf{u}} \\ \mathbf{0}_{\mathbf{u}} & \cdots\cdots & \cdots & \cdots & \cdots & \mathbf{0}_{\mathbf{u}} & \widetilde{\mathbf{F}}_{\mathbf{u},N} \end{pmatrix},$$

(22a)

$$\widetilde{\mathbf{F}}_{\phi,\text{mELY}} = \begin{pmatrix} \widetilde{\mathbf{F}}_{\phi,1} & \mathbf{0}_\phi & \cdots & \mathbf{0}_\phi \\ \mathbf{0}_\phi & \ddots & \ddots & \vdots \\ \vdots & \ddots & \ddots & \mathbf{0}_\phi \\ \mathbf{0}_\phi & \cdots & \mathbf{0}_\phi & \widetilde{\mathbf{F}}_{\phi,N} \end{pmatrix}, \qquad (22b)$$

where $\widetilde{\mathbf{F}}_{\text{mELY}} \in \mathbb{R}^{N(n+m)\times r}$ and $\widetilde{\mathbf{F}}_{\phi,\text{mELY}} \in \mathbb{R}^{Nn\times r}$ are the factors of a system with N stacks and $\mathbf{0}_x \in \mathbb{Z}_{=0}^{n\times r}$ and $\mathbf{0}_u \in \mathbb{Z}_{=0}^{m\times r}$ and $\mathbf{0}_\phi \in 0^{n\times r}$ are zero matrices. For each stack i the corresponding factors $\widetilde{\mathbf{F}}_{\mathbf{x},i}$, $\widetilde{\mathbf{F}}_{\mathbf{u},i}$, and $\widetilde{\mathbf{F}}_{\phi,i}$ are generated as given by (8) and (9).

Remark: While doing the appending of $\widetilde{\mathbf{F}}_{\text{mELY}}$, the order for the states and inputs must be maintained, such that all factor matrices for the states $\widetilde{\mathbf{F}}_{\mathbf{x},N}$ and then the factor matrices for the inputs $\widetilde{\mathbf{F}}_{\mathbf{u},N}$ are appended first. It can be seen, that these matrices contain several zeros which are not needed to describe the system behavior. Here, we can make use of the sparsity to reduce memory requirements.

5 SIMULATION RESULTS

In this section, the simulation results of the eMTI electrolyzer model individually and the mELY operation are presented.

5.1 Electrolyzer Individual Operation

To display the advantage of eMTI class, one electrolyzer stack model is compared to LTI and nonlinear simulation in Figure 4. The whole operation range over the planned 10 years electrolyzer lifetime is reproduced by cycling the input current from $0\,to\,100$ % of the nominal loads current at no degradation ($i_{\text{nom}} = 429.87$ A, for 46 kW stack power with 0 % degradation). In a real operation the cycling would happen much faster and arbitrarily, according to renewable energy production. Neverthe-

less, for this demonstration the extended constant current input operation periods allow seeing the effects of degradation more clearly. The degradation is in a range between 0 % at BoL and 100 % at the estimated EoL, as described in subsection 3.3. As it can be observed in Figure 4 (b), the model can also display operation after EoL. Overall, the output variables of the eMTI model follow the nonlinear behavior over time, with a stronger deviation at the lower boundaries of the operation range. This could be caused by the increased range of the upper bounds to 150 % for the multilinearization. The accuracy of the linear approximation is very good in the beginning at the linearization point, but deviates at partial load, which is getting worse over time.

The states were also analyzed, which are not displayed here for brevity. According to the degradation caused rise of overpotentials, the change in temperature is increasing during fast load changes, which can roughly be represented either by the LTI and eMTI model. The requirement for standard Nafion^{TM} membranes to stay below 90 °C (Christoph Edler, 2018) is fulfilled at any time.

5.2 Multi-stack Electrolyzer Operation

For the mELY operation of 100 stacks, wind data has been used to produce a power profile. The wind data of the year 2021 was taken from a measuring station at 110 m height on the Fraunhofer IWES test field in Bremerhaven, with a sample rate of 10 min. By using an Enercon E-115 2.500 (2.5 MW) power curve, the wind data was translated to the power profile. Afterwards, it was scaled up to fit the 4.6 MW power demand of the mELY at nominal load (0 % degradation). For both operation modes, the same power data was used as input to the main controller. Also, the initial degradation value was set from $0 to 50$ % linearly so that the 1st stack (sELY$_1$) is not degraded at the beginning and the 100th (sELY$_{100}$) stack is degraded by 50 %. In Table 1, the mean electrolyzer efficiency over the whole year is compared. If $p_{ref} = 0$, the efficiency value is not considered for the mean value calculation. The degradation gain of the entire plant in Table 1 is a mean value of all stacks.

Table 1: Comparison of two control modes for the power distribution of a 100 stack mELY operation (one year).

Mode	$\eta_{ely,mean}$ in %	Degradation gain in %
1 - equal	86.78	9.61
2 - max	82.33	9.35

The mean efficiency of mode 1 is higher, as can be observed for the 100 stacks in Figure 5. Since mode 1 results into long periods of partial load operation this behavior is reasonable. This can also be the reason for the increased efficiency of sELY$_{86}$ and sELY$_{100}$ in mode 2. The mean plant degradation gain is 0.26 % less for mode 2. Theoretically, with the linear degradation model and the same overall current input, the degradation gain should be the same for both modes. The deviation can result from the inaccuracy of the controller and degradation models. In Figure 6, different aging rates can be observed for sELY$_1$, sELY$_{50}$ and sELY$_{100}$, showing a correlation of the degradation slope and the individual stack load.

To perform the simulation an S-Function was implemented using a MATLAB-file. For the simulation settings, a fixed time-step was used with automated solver detection and $T_s = 36.9$ s, which represents the fastest dynamics of the electrolyzer. The overall run time of the simulation was 2.81 h using MATLAB R2021b. The simulations are performed on a computer equipped with an Intel®Core™ i7-9850H CPU @ 2.60GHz and 16 GB RAM.

6 DISCUSSION

In this section, the eMTI model accuracy and the mELY simulation results are evaluated.

6.1 Multilinear Model Accuracy

Regarding the individual models for the electrolyzer controller, degradation, and main controller, no multilinear approximation was needed, since the systems are either linear or multilinear right away. However, when combining the submodels to the overall sELY model, an approximation was performed to improve computational time.

To generate the eMTI electrolyzer model approximation, the projection method was used. Overall, regarding the electrolyzer model accuracy, the following basic statements can be made:

- the eMTI model is more accurate than the LTI model over the total operating range,
- the LTI model is exact at operational current with no degradation (linearization point),
- the LTI model cannot handle model changes due to degradation,
- the eMTI model accuracy is rated as sufficient for this application.

For future improvements, a reasonable strategy would be to re-linearize after a certain amount of time
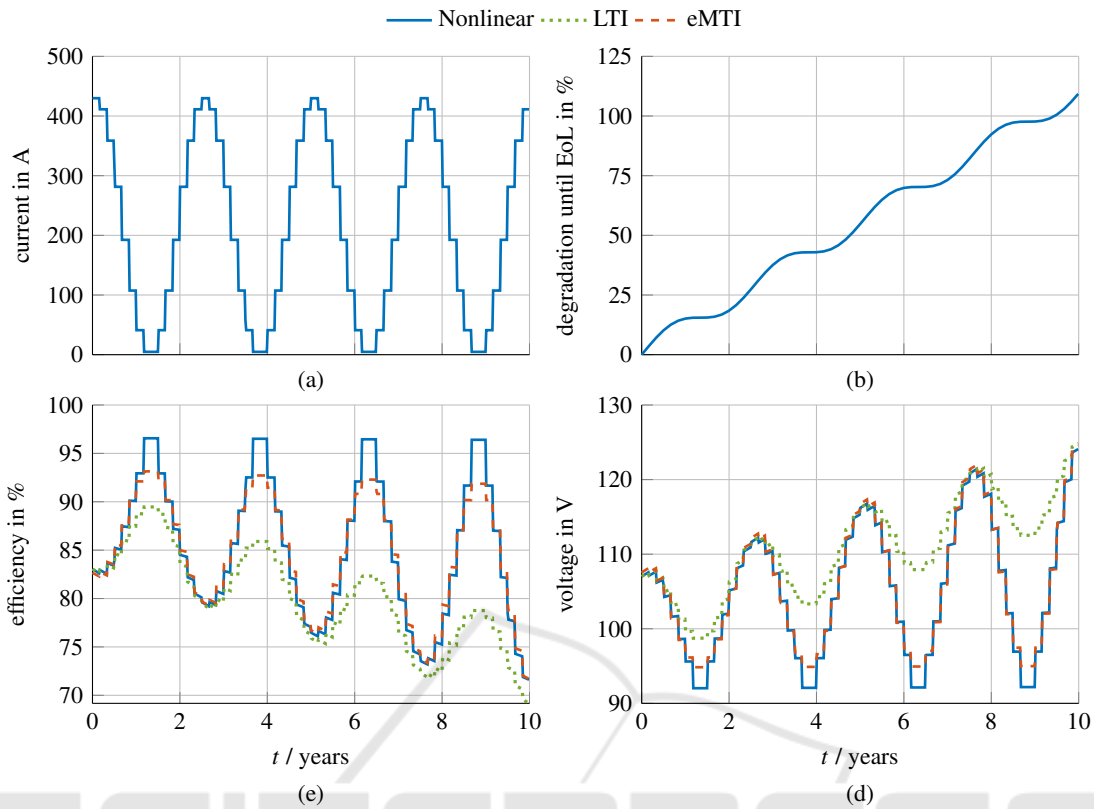
Figure 4: Individual electrolyzer operation for comparison of LTI, eMTI and nonlinear simulation.
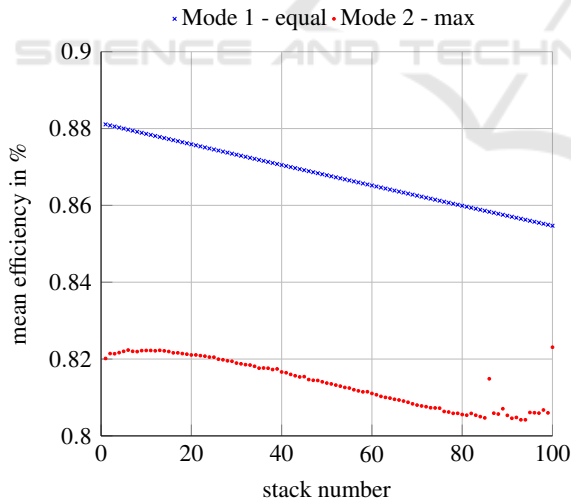

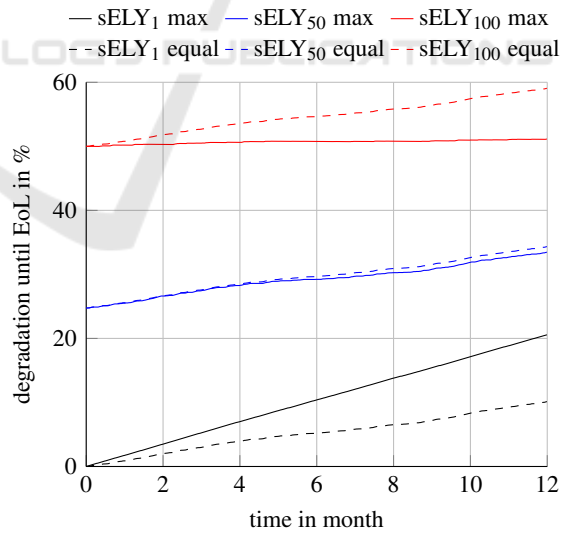Figure 5: Mean values for the individual stack efficiency over one year of operation.

Figure 6: Comparison of degradation for 3 of 100 stacks over one year of operation.

(degradation), wherefore the LTI model stays more accurate over time. Nevertheless, this would not make up for low performance of the LTI model in partial load. Therefore, a combination of LTI and eMTI representation is considered optimal, which can even be combined in a single MTI system, by switching from

eMTI to LTI near the operational point. A different option to enhance the accuracy of the eMTI representation would be to implement a weighting function to the projection method, such that the approximation at the nodes near nominal load is considered more im-

portant (Kruppa et al., 2014). This would at the same time mean a reduced accuracy at the other nodes of the grids, representing the operation range. Overall, the eMTI electrolyzer model accuracy can be considered sufficient for this simulation task.

6.2 Multi-stack Electrolyzer Operation

The results in subsection 5.2 show a clear influence of the main controller operation mode on the mELY performance. With the same total power input and simply changing the power distribution to the stacks, the efficiency can be enhanced. By including more complex degradation phenomena also overall degradation could be prevented. Therefore, this model provides a base for a large optimization problem, with various options for the cost function, e.g., the total economic benefit of the plant from BoL to EoL or sustainable hydrogen production. Therefore, the degradation model needs to be developed further, since there is no influence of, e.g., temperature, dynamic load changes or start-stop events included yet. By also considering the effect of load changes on aging, it could be beneficial for specific stacks to buffer the dynamic behavior.

The mELY model is built by appending the eMTI models. This can be achieved by extending the append function from MATLAB for the MTI class. This process is considerably simpler than constructing mELY with general nonlinear models in Simulink.

Modeling of the mELY in a single eMTI model makes a further tensor decomposition possible, which results in reduced memory and computational resources for the simulation. However, the decomposition method must be chosen carefully, as the structural zeros are removed due the factorization. This can lead to inaccurate decompositions. An analysis of appropriate decomposition methods will be part of future work. In addition, implementing the S-Function in C instead of using a MATLAB-file will increase the simulation speed significantly.

7 CONCLUSIONS

In this paper, a modeling and simulation framework for an mELY operation has been developed. For this purpose, a single electrolyzer stack eMTI model, with degradation input was thoroughly tested. The introduced eMTI electrolyzer model has shown sufficient accuracy for the application. The nonlinear behavior and the dynamics of the mELY could be represented by the eMTI model for the whole operation range. However, modeling errors of the eMTI class could be larger than for general nonlinear representation.

By including the append connector into the MTI model class, the combination of 100 sELY units with individual degradation and power controller model could be done automatically. The performed model reduction methods on the eMTI system were essential to reduce computational cost and generate output data for one year. The output data of the mELY operation showed that different control schemes have a strong influence on the overall electrolyzer efficiency. A similar effect can be observed in the single stack level, where the degradation gain changes with the load profile of each control concept.

In general, eMTI models are suitable to represent energy systems with large number of states. This enables the implementation of modern model-based control methods. By this work, the MTI model class has been further established for engineering applications. This is important since the promising MTI tools are not part of general educational programs, or as well-tried as linear or nonlinear tools yet.

For future work, an electrolyzer model with improved accuracy, by either using a weighting function or a combination with an LTI model, will be pursued. Also, there are numerous options for further simulation performance enhancement, like the use of different tensor decomposition methods for finding low rank approximations or the implementation of the S-Function in C. Prospectively, the submodels can be improved and easily exchanged. To upgrade the degradation model, observers can be used with accelerated stress test data, to find further correlations between aging, current, temperature, pressure, and load changes. For the electrolyzer efficiency, the ancillary components can be considered, as well as a minimum load range. Also, an option for overload could be included, with consideration of heat and hydrogen flow management limitations. This can be implemented in a main advanced feedback controller model. By considering the degradation state and efficiency feedback, the main controller could perform a multi-criteria optimization. Overall, this modeling approach sets the base for various further developments, while also serving as a controller test bench. Future studies are currently focused in mELY power distribution operation schemes, which can be implemented by electrolyzer operators for a larger return of invest and plant lifetime.

ACKNOWLEDGEMENTS

REFERENCES

Agora Energiewende and Guidehouse (2021). Making renewable hydrogen cost-competitive: Policy instruments for supporting green H_2.

Bahr, M., Gusak, A., Stypka, S., and Oberschachtsiek, B. (2020). Artificial neural networks for aging simulation of electrolysis stacks. *Chemie Ingenieur Technik*, 92(10):1610–1617.

Bro, R. and Kiers, H. A. (2003). A new efficient method for determining the number of components in parafac models. *Journal of Chemometrics: A Journal of the Chemometrics Society*, 17(5):274–286.

Buttler, A. and Spliethoff, H. (2018). Current status of water electrolysis for energy storage, grid balancing and sector coupling via power-to-gas and power-to-liquids: A review. *Renewable and Sustainable Energy Reviews*, 82:2440–2454.

Christoph Edler (2018). Untersuchung der Einsatzmoeglichkeiten von Hochleistungselektrolyseuren fuer Netzdienstleistungen. diploma thesis, TU Wien, https://repositum.tuwien.at/handle/20.500.12708/7708.

Cihlar, J., Villar Lejarreta, A., Wang, A., Melgar, F., Jens, J., and Rio, P. (2020). Hydrogen generation in europe: Overview of costs and key benefits. Luxembourg. Publications Office of the European Union.

Enapter (2022). The AEM Multicore: Lowest-Cost Flexible Hydrogen at Megawatt-Scale. https://www.enapter.com/aem-multicore, Accessed: 28.02.2022.

Espinosa-López, M., Darras, C., Poggi, P., Glises, R., Baucour, P., Rakotondrainibe, A., Besse, S., and Serre-Combe, P. (2018). Modelling and experimental validation of a 46 kW PEM high pressure water electrolyzer. *Renewable Energy*, 119:160–173.

Frensch, S. H., Fouda-Onana, F., Serre, G., Thoby, D., Araya, S. S., and Kær, S. K. (2019). Influence of the operation mode on PEM water electrolysis degradation. *International Journal of Hydrogen Energy*, 44(57):29889–29898.

Geitmann, S. (2022). HZwei - Das Magazin für Wasserstoff und Brennstoffzellen. Hydrogeit Verlag. Issue 1, January 2022.

Green Hydrogen Systems (2022). HyProvide™: A-Series. https://greenhydrogensystems.com/wp-content/uploads/2021/02/A-Series-brochure-120421.pdf, Accessed: 28.02.2022.

H-TEC SYSTEMS GmbH (2022). H-TEC PEM-Elektrolyseur ME450/1400. https://www.h-tec.com/produkte/detail/h-tec-pem-elektrolyseur-me450-1400/me450-1400/, Accessed: 17.03.2022.

Hornik, K., Stinchcombe, M., and White, H. (1989). Multilayer feedforward networks are universal approximators. *Neural Networks*, 2(5):359–366.

IRENA (2020). Green Hydrogen Cost Reduction: Scaling up Electrolysers to Meet the 1.5°C Climate Goal. International Renewable Energy Agency. Abu Dhabi.

Kolda, T. G. (2006). Multilinear operators for higher-order decompositions. Technical report, Citeseer.

Kopp, M., Coleman, D., Stiller, C., Scheffer, K., Aichinger, J., and Scheppat, B. (2017). Energiepark Mainz: Technical and economic analysis of the world-wide largest Power-to-Gas plant with PEM electrolysis. *International Journal of Hydrogen Energy*, 42(19):13311–13320.

Kosonen, A., Koponen, J., Huoman, K., Ahola, J., Ruuskanen, V., Ahonen, T., and Graf, T. (2016). Optimization strategies of PEM electrolyser as part of solar PV system. In *2016 18th European Conference on Power Electronics and Applications (EPE'16 ECCE Europe)*, pages 1–10. IEEE.

Kruppa, K. (2018). *Multilinear Design of Decentralized Controller Networks for Building Automation Systems*. PhD thesis, HafenCity Universität Hamburg.

Kruppa, K., Pangalos, G., and Lichtenberg, G. (2014). Multilinear approximation of nonlinear state space models. *IFAC Proceedings Volumes*, 47(3):9474–9479.

Lichtenberg, G., Pangalos, G., Cateriano Yáñez, C., Luxa, A., Jöres, N., Schnelle, L., and Kaufmann, C. (2022). Implicit multilinear modeling. *at - Automatisierungstechnik*, 70(1):13–30.

P. Ayivor, J. Torres, M.A.M.M. van der Meijden, R. van der Pluijm, and B. Stouwie (2018). Modelling of large size electrolyzer for electrical grid stability studies in real time digital simulation. *IEEE*.

Pangalos, G., Eichler, A., and Lichtenberg, G. (2013). Tensor systems - multilinear modeling and applications. *3rd International Conference on Simulation and Modeling Methodologies, Technologies and Applications (SIMULTECH-2013)*, pages 275–285.

Rakousky, C., Reimer, U., Wippermann, K., Kuhri, S., Carmo, M., Lueke, W., and Stolten, D. (2017). Polymer electrolyte membrane water electrolysis: Restraining degradation in the presence of fluctuating power. *Journal of Power Sources*, 342:38–47.

Schnelle, L., Lichtenberg, G., and Warnecke, C. (2022). Using low-rank multilinear parameter identification for anomaly detection of building systems. *11th IFAC Symposium on Fault Detection, Supervision and Safety for Technical Processes*. Status: accepted.

The MathWorks, Inc. (2022). append - Group models by appending their inputs and outputs. https://de.mathworks.com/help/control/ref/lti.append.html, Accessed: 16.03.2022.

Zagorowska, M., Wu, O., Ottewill, J. R., Reble, M., and Thornhill, N. F. (2020). A survey of models of degradation for control applications. *Annual Reviews in Control*, 50:150–173.